Monthly Notices of the ROYAL ASTRONOMICAL SOCIETY

Mon. Not. R. Astron. Soc. **420,** 1621–1629 (2012) doi:10.1111/j.1365-2966.2011.20155.x

Cluster–cluster lensing and the case of Abell 383

Adi Zitrin,[1★] Yoel Rephaeli,[1] Sharon Sadeh,[1] Elinor Medezinski,[2] Keiichi Umetsu,[3] Jack Sayers,[4] Mario Nonino,[5] Andrea Morandi,[1] Alberto Molino,[6] Nicole Czakon[4] and Sunil R. Golwala[4]

[1] *School of Physics and Astronomy, The Raymond and Beverly Sackler Faculty of Exact Sciences, Tel Aviv University, Tel Aviv 69978, Israel*
[2] *Department of Physics and Astronomy, The Johns Hopkins University, 3400 North Charles Street, Baltimore, MD 21218, USA*
[3] *Institute of Astronomy and Astrophysics, Academia Sinica, PO Box 23-141, Taipei 10617, Taiwan*
[4] *Division of Physics, Mathematics, and Astronomy, California Institute of Technology, Pasadena, CA 91125, USA*
[5] *INAF-Osservatorio Astronomico di Trieste, Via Tiepolo 11, I-34131 Trieste, Italy*
[6] *Instituto de Astrofísica de Andalucía (CSIC), C/Camino Bajo de Huétor 24, Granada 18008, Spain*

Accepted 2011 November 7. Received 2011 October 28; in original form 2011 August 24

ABSTRACT

Extensive surveys of galaxy clusters motivate us to assess the likelihood of cluster–cluster lensing (CCL), namely, gravitational lensing of a background cluster by a foreground cluster. We briefly describe the characteristics of CCLs in optical, X-ray and Sunyaev–Zel'dovich effect measurements, and calculate their predicted numbers for Λ cold dark matter (ΛCDM) parameters and a viable range of cluster mass functions and their uncertainties. The predicted number of CCLs in the strong-lensing regime varies from several (<10) to as high as a few dozen, depending mainly on whether lensing triaxiality bias is accounted for, through the c–M relation. A much larger number is predicted when taking into account also CCL in the weak-lensing regime. In addition to few previously suggested CCLs, we report a detection of a possible CCL in A383, where background candidate high-z structures are magnified, as seen in deep Subaru observations.

Key words: galaxies: clusters: general – galaxies: clusters: individual: Abell 383 – cosmology: observations – dark matter.

1 INTRODUCTION

The mass density in the central regions of galaxy clusters typically exceeds the critical value required for lensing, generating multiple images of background objects. This phenomenon is known as strong lensing (SL) and the background sources are usually very distant field galaxies, lensed into magnified and often multiple arcs on the lens plane. Recent analyses have shown that many sets of multiply-lensed images can be uncovered with high-quality space imaging measurements and improved modelling techniques (e.g. Broadhurst et al. 2005; Liesenborgs et al. 2007; Limousin et al. 2008; Newman et al. 2009; Zitrin et al. 2009; Coe et al. 2010; Deb et al. 2010; Richard et al. 2010; Merten et al. 2011).

With more precise knowledge of the global and large-scale parameters, and extensive ongoing surveys of galaxy clusters in several spectral regions, the possibility of a foreground cluster lensing a background cluster is of practical interest.

An initial estimate of the possibility of observing cluster–cluster lensing (CCL) was made by Cooray, Holder & Quashnock (1999), who predicted that a few dozen CCLs maybe observed over the full sky. Soon thereafter, two such lenses were discovered. Blakeslee (2001) and Blakeslee et al. (2001) found that the nearby supercluster A2152 ($z = 0.043$) is actually a chance alignment of two clusters: A2152 and a more massive background cluster at $z = 0.134$ (which was then designated A2152-B). The centres of these two clusters are separated by 2.4 arcmin, and some background cluster galaxies of the more distant cluster seem magnified and distorted in the image plane of A2152. Athreya et al. (2002) have shown that an excess of distant galaxies in the south-west area of MS 1008−1224 is most likely also a weaker lensing effect of a background cluster near the line of sight. Two other clusters seem to lens very small groups of galaxies: in addition to the many images seen across its field, A1689 lenses a galaxy group of three members at $z_S = 1.83$ (Limousin et al. 2007, see also Broadhurst et al. 2005), and A2218 also lenses a three-member group at $z_S = 2.515$ (Elíasdóttir et al. 2007). There seem to be no other explicit cases of CCLs reported to date.

Bertin & Lombardi (2001) have also investigated the properties of a 'double lens' configuration, and mainly its effect on weak-lensing (WL) analyses. In this context, the effect of interest is the lensing of a background source by two (at least partially) aligned lenses, where several such configurations were suggested or theoretically discussed before (e.g. Crawford, Fabian & Rees 1986; Seitz &

★E-mail: adiz@wise.tau.ac.il

Schneider 1994; Molinari, Buzzoni & Chincarini 1996; Wang & Ulmer 1997; Gavazzi et al. 2008).

Major advances in the capability of detecting weak low-brightness emission in the optical and X-ray regions, and more recently also in Sunyaev–Zel'dovich (SZ; Sunyaev & Zel'dovich 1970) effect mapping of many clusters, together with increased precision in the values of the cosmological parameters, make the (strong) CCL phenomenon of practical interest as a probe of cluster properties. Additionally, the statistics of CCLs enhances the use of clusters as probes of the evolution of the large-scale structure (LSS). The manifestation of SL in different bands of the electromagnetic spectrum secures the identification of CCLs. Contrasting the results from a search of CCLs with theoretical predictions may yield important new insight, especially on the late evolution of the LSS.

We briefly describe the possible observational signatures of CCLs in the optical, X-ray and SZ measurements, and carry out a detailed calculation of the expected numbers of CCLs in several cosmological models using current values of the global and cluster parameters. Our updated treatment here (for previous calculation see Cooray et al. 1999) yields a wide range of values for the predicted numbers of CCLs, reflecting modelling and observational uncertainties. Additionally, we report a (possible) discovery of another moderately lensed (magnified by 14 ± 3 per cent; see Section 4), high-z background cluster at $z \sim 0.9^{+0.2}_{-0.1}$ behind A383 ($z = 0.19$), $\sim$2.5 arcmin from its centre.

The paper is organized as follows. In Section 2 we discuss the observational properties of CCL. In Section 3 we present our calculation of the probability for CCLs and their predicted numbers. The possible detection of a CCL in the field of A383 is discussed in Section 4. Our main results are summarized in Section 5.

2 OBSERVATIONAL PROPERTIES OF CCLs

Lensing of a background cluster results in magnified optical images of the background cluster galaxies, and in hitherto undetected signatures in the X-ray and microwave regions. In the image plane, a clear local overdensity of magnified, distorted and stretched optical images would generally be expected when the galaxies of a background cluster are lensed. The higher redshift of the background cluster should result in images fainter by the luminosity–distance ratio (relative to the lensing cluster), but boosted by the magnification effect which though preserves surface brightness, will magnify the total flux (due to the increased area occupied by each source in the image plane). Also, when having multiband imaging, the higher redshift of the background cluster will cause the background galaxies to look redder relative to the lens red-sequence galaxies, though this effect might not be prominent in a simple RGB colour-composite image when redshift differences are relatively small (and further weakened by the Butcher–Oemler effect; e.g. Butcher & Oemler 1978), and in such a case are more likely to be revealed by producing photometric catalogues which may exhibit a different, secondary red sequence corresponding to the background cluster.

Another property which may allow for an optical detection of CCLs lies in the relation between the effective radius of cluster ellipticals to their surface brightness, often referred to as the Kormendy relation (or the Fundamental Plane if velocity dispersion is also accounted for; Kormendy 1977; Djorgovski & Davis 1987; Kormendy & Djorgovski 1989). The magnification by the foreground object should in practice increase the measured half-light or effective radius of each background cluster member, while preserving surface brightness (Bertin & Lombardi 2006; Sonnenfeld, Bertin & Lombardi 2011). When the magnification is high enough, a shift from the standard Kormendy relation, obtained from other unmagnified clusters at a redshift of the background cluster, should be noticed. This in fact maybe useful for searching prominent cases of CCL in large sky surveys.

The steep dependence of the X-ray surface brightness on redshift would generally mean that, even though magnified by the foreground cluster, the background cluster will at best look as a faint part of the foreground cluster emission. If the background cluster lies further away from the line of sight, there might be a traceable signature, as the magnified background flux will be seen far enough from the foreground cluster centre, where the foreground flux is lower and thus might enable a clear detection, but only if the background cluster is sufficiently luminous. We note, however, that in the strong regime this may resemble X-ray images of a substructure, merger or related shocks, and thus without additional information; even if such a signal is detected it could well be misinterpreted. In addition (as was noted previously by Cooray et al. 1999), X-ray spectra can be used to determine the background cluster redshift, particularly by the measurement of the relatively strong Fe lines. Current measurement capabilities (e.g. with *Chandra*) enable determining the cluster redshift up to $z \sim 1$. Still, it might not be feasible to detect a CCL based solely on X-ray imaging measurements.

The SZ effect is the change in the cosmic microwave background (CMB) intensity due to Compton scattering of CMB photons as they traverse intracluster gas (e.g. Rephaeli 1995; Carlstrom, Holder & Reese 2002). The result is a redshift-independent distortion of the CMB spectrum, whose thermal component constitutes a decrement of CMB spectrum below $\simeq$218 GHz, and an increment of the spectrum above $\simeq$218 GHz.

The SZ effect is measured with respect to the unscattered CMB at the location of the cluster, so lensing affects the SZ signal similarly at all observed frequencies. The total observed SZ signal is therefore a sum of the intrinsic SZ signal from the lensed cluster, which is then magnified by the foreground cluster, plus the SZ signal due to scattering in the foreground cluster.

The fact that the SZ effect is independent of redshift may help in making the identification of a CCL more feasible in SZ surveys than in X-ray surveys. However, it may still be hard to disentangle the signals of the foreground and background structures, as the SZ signal usually stretches out to large (projected) distances and may thus cover up lensed features. The net result from such a trade-off will depend on the lens and source redshifts, and on the projected distance of the lensed feature from the line of sight of the lensing cluster, so that generally, structures closer to the line of sight will be more strongly lensed and magnified, but the relative flux from the foreground cluster will also be higher. As in the X-ray, strong CCL here may also resemble images of merger, or related shocks. Obviously, a CCL identification can be more secure if lensing features are revealed in both X-ray and SZ measurements, or if clearly detected in optical imaging measurements. With photometric and/or spectroscopic data, such a detection could yield precise information on both clusters.

In Section 4 we elaborate further on the lensing signatures in the optical, X-ray and SZ regions, as manifested in A383, which seems to be moderately lensing a background cluster.

3 PREDICTED NUMBERS OF CLUSTER–CLUSTER LENSES

In order to assess the probability for CCLs we integrate the mass function over two cluster populations, namely those of the lenses and sources. We do so for both the (Press & Schechter 1974, hereafter PS) mass function, and that of (Sheth & Tormen 1999, hereafter ST). For each cluster of the lens population we integrate the mass function of sources lying behind the lens, and included within the Einstein radius, as (properly) determined by the source and lens redshifts. The volume element over which the source integration is carried out is computed in terms of the solid angle defined by the Einstein ring in the plane of the lens, projected on to the source redshift, by means of the ratio of the squared lens–source angular diameter distances. Sources within this volume element will be lensed or deflected to appear up to approximately twice the Einstein radius in the image plane, which we take here as the SL region. Integrating over the lens population then yields the desired number of CCLs.

One should note that in practice, due to the magnification, the critical curve and the area subtended by it project back to a smaller area in the source plane. Sources that lie inside the caustics will be multiply-lensed, while sources close to but outside the caustics will only be deflected, so that the actual position of the source is closer to the central line of sight than actually observed. Clearly, the actual lensing pattern depends on the projected mass profile of the lens and the relevant distances, but it can be shown (from simple geometric considerations) that for roughly similar observer–lens and lens–source distances, approximately twice the Einstein radius in the image plane corresponds to the radius of the SL region in the source plane (see also Fig. 1). Similarly, since SL occurs in the central region where the (3D) density slope is shallow, say, close to isothermal ($\mathrm{d}\ln[\rho]/\mathrm{d}\ln[r] = -2$), then the deflection angle is $\sim$constant, so that $\Delta\beta[\mathrm{SL}] \simeq \Delta\theta[\mathrm{SL}] \simeq 2\theta_{\mathrm{E}}$. Thus, sources that lie within this circle in the source plane would appear usually up to twice the Einstein radius in the image plane. Since the magnification at twice the Einstein radius is usually already small (say, a magnification of few or less), this is a reasonable approximation for our purposes here.

Note that we include in this estimate only sources that are fully enclosed within the respective Einstein radius, ignoring a partial alignment of the source within this radius. In this regard our estimate constitutes a lower limit on the number of CCLs.

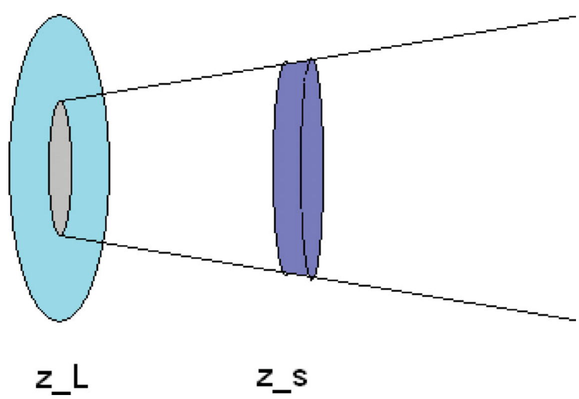

Figure 1. The lens–source configuration. The grey area represents the section of the lens plane which is included within the Einstein radius, as calculated from the lens and source redshifts. Integration of the source population is performed along the cone extending to the right of the lens, with an angular cross-section corresponding to the projected Einstein radius at the source redshift, z_{S}. The corresponding source-plane volume element is denoted in purple. Note that by virtue of the low angular scales involved, one can safely use the flat-sky approximation to calculate the volume element at the source redshift.

3.1 Method

The equation governing the relation between the concentration parameter and the Einstein radius assuming an (Navarro, Frenk & White 1996, hereafter NFW) profile (Broadhurst & Barkana 2008) is

$$\left(\frac{4R_{\mathrm{v}}\rho_{\mathrm{c}}^{z}\Delta_{\mathrm{c}}}{3\Sigma_{\mathrm{cr}}}\right)\frac{c_{\mathrm{v}}^{2}}{\ln(1+c_{\mathrm{v}})-c_{\mathrm{v}}/(1+c_{\mathrm{v}})}\frac{g(x)}{x^{2}} = 1, \tag{1}$$

where Δ_{c} and ρ_{c}^{z} are the overdensity at virialization and critical density at redshift z, respectively,

$$\Sigma_{\mathrm{cr}} = \frac{c^{2}}{4\pi G}\frac{D_{\mathrm{OS}}}{D_{\mathrm{OL}}D_{\mathrm{LS}}} \tag{2}$$

is the critical surface density, D_{OS}, D_{OL} and D_{LS} are the observer–source, observer–lens and lens–source distances, respectively, and

$$R_{\mathrm{v}} = \frac{1.69}{1+z}\left[\frac{M}{M_{15}}\frac{18\pi^{2}}{\Omega_{\mathrm{m}}\Delta_{\mathrm{c}}(\Omega_{\mathrm{m}}, z)}\right]^{1/3}\ \mathrm{Mpc}\,h^{-1}, \tag{3}$$

is the virial radius. Also, $x \equiv (R_{\mathrm{E}}c_{\mathrm{v}})/R_{\mathrm{v}}$, where R_{E} is the Einstein radius, and

$$g(x) = \ln\frac{x}{2} + \begin{cases} 1, & x = 1 \\ \frac{2}{\sqrt{x^{2}-1}}\tan^{-1}\sqrt{\frac{x-1}{x+1}}, & x > 1 \\ \frac{2}{\sqrt{1-x^{2}}}\tanh^{-1}\sqrt{\frac{1-x}{1+x}}, & x < 1 \end{cases}. \tag{4}$$

The concentration parameter c_{v} scales with mass and redshift according to the following relation:

$$c_{\mathrm{v}} = A(M/M_{*})^{B}(1+z)^{C}, \tag{5}$$

where the parameters A, B, C and M_{*} are taken from various c–M relations as we discuss below.

The solution of equation (1) provides the Einstein radius as a function of c_{v}, from which the angular Einstein radius $\theta_{\mathrm{E}} = R_{\mathrm{E}}/D_{\mathrm{A}}(z_{\mathrm{L}})$, the ratio between the (physical) Einstein radius and the angular diameter distance to the lens, can be readily determined.

Having solved for the angular Einstein radius at the lens, we can now estimate the number of source clusters that would be strongly lensed, i.e. the ones lying behind the lens and included within the angular area subtended by the Einstein radius. For this purpose we set the lens mass and redshift, and integrate the mass function over the relevant mass range, a volume element defined by the source-cluster redshift, $z_{\mathrm{L}} < z_{\mathrm{S}} < \infty$, and the angular diameter element specified by the Einstein radius of the lens–source system, projected on to the source redshift by means of the squared lens–source angular diameter distance ratio, $(d_{\mathrm{A_L}}/d_{\mathrm{A_S}})^{2}$ (Fig. 1). This result provides the number of lensed sources behind a lens lying at redshift z_{L}, and having a mass m_{L}. The total number of CCL occurrences is likewise estimated by integrating the mass function over the mass–redshift space of the lens:

$$\begin{aligned} N_{\mathrm{cc}} &= \int_{m_{\mathrm{L}}}\int_{V_{\mathrm{L}}}\int_{m_{\mathrm{S}}}\int_{V_{\mathrm{S}}} n(m_{\mathrm{L}}, z_{\mathrm{L}})n(m_{\mathrm{S}}, z_{\mathrm{S}})\,\mathrm{d}m_{\mathrm{L}}\,\mathrm{d}V_{\mathrm{L}}\,\mathrm{d}m_{\mathrm{S}}\,\mathrm{d}V_{\mathrm{S}} \\ &= 4\pi\int_{m_{\mathrm{L}}}\int_{z_{\mathrm{L}}} n(m_{\mathrm{L}}, z_{\mathrm{L}})r_{\mathrm{L}}^{2}\mathrm{d}m_{\mathrm{L}}\frac{\mathrm{d}r_{\mathrm{L}}}{\mathrm{d}z_{\mathrm{L}}}\,\mathrm{d}z_{\mathrm{L}}\cdots \\ &\quad\times\cdots\int_{m_{\mathrm{S}}}\int_{z_{\mathrm{S}}}\int_{\Omega_{\theta_{\mathrm{E}}}} n(m_{\mathrm{S}}, z_{\mathrm{S}})\,\mathrm{d}m_{\mathrm{S}}\,\mathrm{d}z_{\mathrm{S}}\,\mathrm{d}\Omega_{\theta_{\mathrm{E}}}. \end{aligned} \tag{6}$$

3.2 Results

As is obvious, results depend significantly on the mass function, and quite strongly on the c–M relation. This relation is only roughly estimated from numerical simulations of clusters; therefore, it introduces a large uncertainty in the predicted numbers of CCLs. We have used the PS and ST mass functions and various *c–M* relations, each specified in terms of a different set of A, B, C and M_* parameters (in equation 5). We first use the notation and parameters given in Komatsu & Seljak (2002), based on the work of Seljak (2000) and Bullock et al. (2001). In this notation $M_* = 5.3 \times 10^{12}\,\mathrm{M}_{\odot}$ [as calculated by us according to 7-year *Wilkinson Microwave Anisotropy Probe* (*WMAP*7) parameters] is the solution to $\sigma(M) = \delta_c$, where $\sigma(M)$ is the present-day rms mass fluctuations, and δ_c is the threshold overdensity for spherical collapse at $z = 0$, with $A = 10$, $B = -0.2$ and $C = -1$.

In a Λ cold dark matter (ΛCDM) cosmological model with (Ω_m, Ω_Λ, n, h, σ_8) = (0.266, 0.734, 0.963, 0.71, 0.801) as taken from *WMAP*7 results, the above parameters for the *c–M* relation, and clusters in the mass interval, 1×10^{13}–$1 \times 10^{16}\,\mathrm{M}_{\odot}$ our calculations yield ∼0.05 CCLs with a PS mass function, and ∼0.2 CCLs with a ST mass function. When taking into account also background groups of galaxies down to $5 \times 10^{12}\,\mathrm{M}_{\odot}$, we obtain ∼0.3 CCLs with a PS mass function and ∼0.8 CCLs with the ST mass function.

We repeated the calculation with the *c–M* relation given by Duffy et al. (2008) for their full sample, in which $M_* = 2 \times 10^{12}\,h^{-1}\,\mathrm{M}_{\odot}$, $A = 7.85$, $B = -0.081$ and $C = -0.71$. With these values, for a ΛCDM model with (Ω_m, Ω_Λ, n, h, σ_8) = (0.258, 0.742, 0.963, 0.719, 0.796) taken from *WMAP*5 results (as used in Duffy et al. 2008), and mass limits of 1×10^{13}–$1 \times 10^{16}\,\mathrm{M}_{\odot}$, our calculations yield around one CCL with a PS mass function and around two CCLs with a ST mass function. When taking into account also background groups of galaxies down to $5 \times 10^{12}\,\mathrm{M}_{\odot}$, our calculations yield around three CCLs with a PS mass function and around eight with a ST mass function. We note that the *c–M* relation presented in Bullock et al. (2001) yields similar results.

In order to take into account the lensing projection bias of triaxial cluster morphology, the calculation was repeated with the *c–M* relation of Hennawi et al. (2007), in which $M_* = 1.3 \times 10^{13}\,h^{-1}\,\mathrm{M}_{\odot}$, $A = 12.3$, $B = -0.13$ and $C = -1$.

For these values, in ΛCDM model with (Ω_m, Ω_Λ, n, h, σ_8) = (0.258, 0.742, 0.963, 0.719, 0.796) taken from *WMAP*5 results, and mass limits of 1×10^{13}–$1 \times 10^{16}\,\mathrm{M}_{\odot}$, our calculations yield around nine CCLs with a PS mass function and ∼17 CCLs with a ST mass function. When taking into account also background groups of galaxies down to $5 \times 10^{12}\,\mathrm{M}_{\odot}$, we predict ∼38 CCLs with a PS mass function and ∼68 CCLs with a ST mass function. Thus, taking into account the lensing projection bias boosts CCL numbers by about an order of magnitude.

We compare these results to the observed *c–M* relation from a small sample of 10 clusters derived by Oguri et al. (2009), in which $M_* = 1 \times 10^{15}\,\mathrm{M}_{\odot}$, $A = 12.4$, $B = -0.081$ and $C = -1$. This relation yields concentrations higher than that predicted by ΛCDM simulations, and even higher than those derived observationally by previous work (e.g. Comerford & Natarajan 2007), and are likely to be extreme results that are perhaps less relevant for our purposes.

Assuming these values, in ΛCDM with (Ω_m, Ω_Λ, n, h, σ_8) = (0.258, 0.742, 0.963, 0.719, 0.796) taken from *WMAP*5 results, and mass limits of $1 \times 10^{13}\,\mathrm{M}_{\odot}$–$1 \times 10^{16}\,\mathrm{M}_{\odot}$, our calculations yield ∼165 CCLs with a PS mass function and ∼260 CCLs with a ST mass function. When taking into account also background groups of galaxies down to $5 \times 10^{12}\,\mathrm{M}_{\odot}$, our calculations yield ∼660 CCLs with a PS mass function and ∼940 CCLs with a ST mass function. Thus, according to the observed relation (which is known to produce higher concentration than ΛCDM simulations) the predicted total numbers of CCLs are quite large.

It should be noted that taking into account the WL regime, in which the background cluster does not have to be within the Einstein radius as projected on to the source plane, but can be further out up to several Einstein radii, the likelihood of a CCL increases significantly. Specifically, still assuming the flat-sky approximation, the likelihood of a CCL increases simply as the square of the ratio of the projected distance of the background cluster and the Einstein radius of the foreground cluster.

Moreover, extending the calculations to the 1σ ranges of the ΛCDM parameters broadens the ranges of our predicted numbers of CCLs by up to a factor of ∼2. Finally, the use of other mass functions – such as Jenkins et al. (2001) or Tinker et al. (2008) – can introduce another ∼20 per cent variation.

4 A383: A NEW CCL

In the course of this work we inspected (among other clusters) deep archival multiband images of A383 obtained with the SuprimeCam on the Subaru telescope (Miyazaki et al. 2002) in 2002, 2005, 2007, 2008 and new data collected in 2010 dedicated to the Cluster Lensing And Supernova survey with Hubble (CLASH) sample (Postman et al. 2011; see also below), with total integration times of at least ∼1 h and up to ∼4 h, for each of the B, V, R_c, I_c, i' and z' bands. Our analysis indicates that this is possibly a new example of a CCL, with the lensed system being either a background cluster or a group of galaxies. Standard image reduction was performed with mscred task in IRAF,[1] while co-added images were created following Nonino et al. (2009). Zero-points were estimated from standard star observations.

In these wide-field (≈30 × 30 arcmin^2) Subaru images of the field of A383, the multiwavelength coverage uncovers several higher z structures. Among these, two large structures are seen; one is located ∼5.2 arcmin east and ∼2.2 arcmin north of A383, around RA = 02:48:24.96, Dec. = −03:29:31.8, and the second ∼13 arcmin east and ∼2.8 arcmin north of A383, around RA = 02:48:56.03 Dec. = −03:29:06.6, and extends northwards towards a third (possibly different) substructure of similar colours (and redshift), but these structures are too far from the centre of A383 to be relevant for this work. Our Bayesian photometric redshift (Benítez 2000; Benítez et al. 2004; Coe et al. 2006) photometric catalogue, based on the six Subaru imaging bands mentioned above, suggests redshifts of $z \sim 0.3$ and 0.7 for these structures, respectively, which further reduces their expected magnification by A383 to ≃1.

The more interesting case we consider here is a clear redder sequence of galaxies, ∼2.5 arcmin north-east of the centre of A383, around RA = 02:48:09.57, Dec. = −03:29:41.6 (see Fig. 2). The background structure is clearly seen as a red overdensity of galaxies very faint in the B band (see Fig. 2 for an RGB colour image), implying a higher redshift than A383, further confirmed by a photometric redshift of $z \sim 0.9^{+0.2}_{-0.1}$ for all 40 member galaxies. The average photometric redshift for these galaxies is $z = 0.96$, though we adopt the photo-z of the brightest member, $z \simeq 0.9$, as the redshift of this structure.

We have downloaded *Chandra* X-ray images and obtained Bolocam 140-GHz SZ images of A383 to examine whether this background cluster is seen also in these spectral regions. As maybe expected (see Section 2), no excess X-ray brightness is seen at the

[1] Valdes (1998). IRAF is distributed by the National Optical Astronomy Observatories, which are operated by the Association of Universities for Research in Astronomy, Inc., under cooperative agreement with the National Science Foundation.

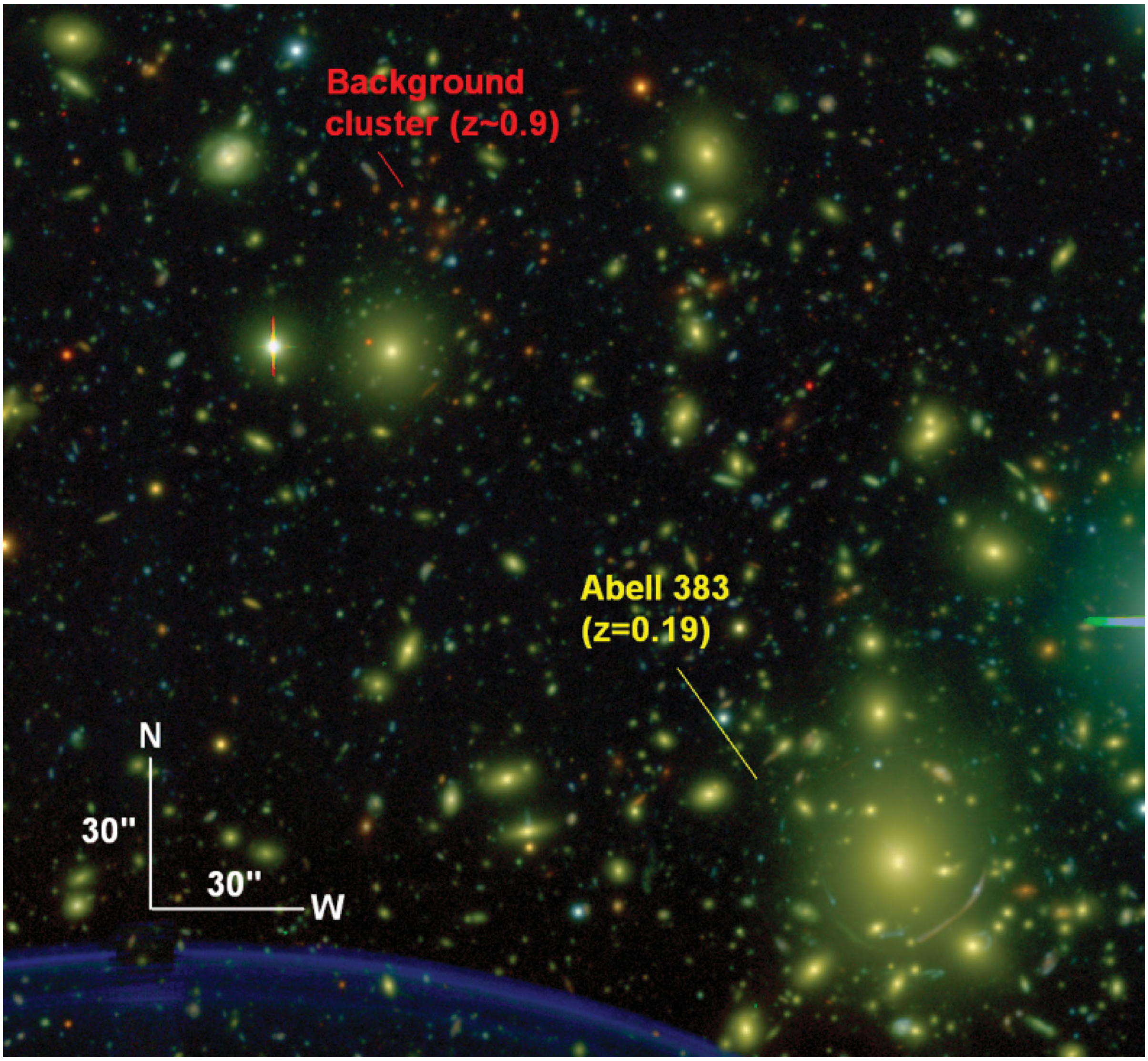

Figure 2. The central field of A383 with the high-z background cluster marked on the image. Note the much redder colours of the galaxies in the background cluster with respect to A383. According to our WL analysis, A383 magnifies the background cluster by 14 ± 3 per cent (see Section 4 for more details).

location of the cluster (see Fig. 3), possibly due to a low-mass (and low-temperature) cluster or group. Neither is the lensed cluster detected in the processed SZ map (see Fig. 4). The optical, SZ and X-ray signals of the lensed cluster are used below to place limits on its mass, along with a WL analysis mass estimation.

A383 is one of 25 clusters covered in the CLASH multicycle treasury programme. The CLASH programme has been awarded 524 orbits of *Hubble Space Telescope* (*HST*) time to conduct a multicycle programme that will couple the gravitational-lensing power of 25 massive intermediate-redshift clusters with *HST*'s newly enhanced panchromatic imaging capabilities (Wide Field Camera 3 and the restored Advanced Camera for Surveys), in order to test structure formation models with unprecedented precision. More details can be found in Postman et al. (2011).

To further base the results of this work, and in the framework of the CLASH collaboration, we have constructed strong and WL models for this field (respectively, Zitrin et al. 2011b and Umetsu et al., in preparation). Interestingly, the different background structures are seen in the wide-field WL analysis, which we use to derive a magnification of 14 ± 3 per cent at the location of the lensed

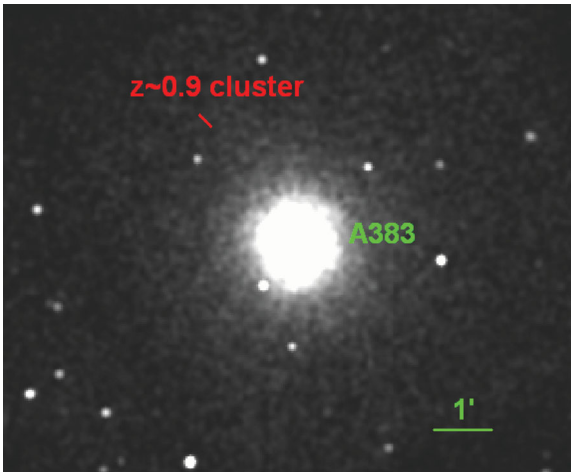

Figure 3. Smoothed X-ray image of A383. The location of the $z \sim 0.9$ background cluster is indicated by the red line. No noticeable excess is seen in that location, as can be expected (see Section 2).

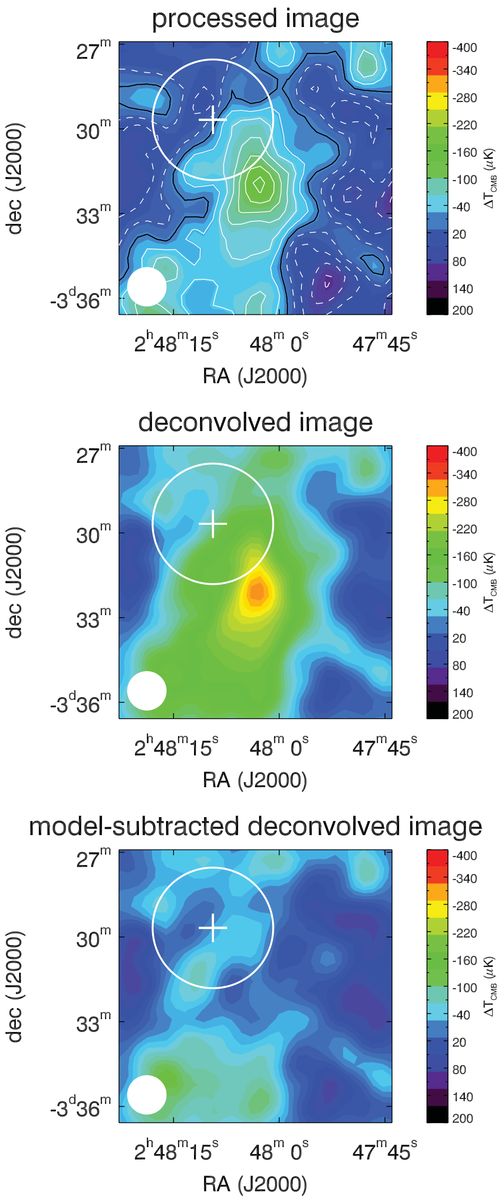

Figure 4. Bolocam SZ images of A383. From top to bottom the thumbnails show the high-pass filtered (processed) image, the deconvolved image and the model-subtracted deconvolved image. The solid white contours in the processed image represent signal-to-noise ratio (S/N) of $-1, -2, -3, \ldots$, and the dashed white contours represent S/N $= +1, +2, +3, \ldots$. We do not include S/N contours in the deconvolved images due to the significant amount of large-angular-scale noise. The white plus sign denotes the centre of the $z = 0.9$ cluster, and the unfilled white circle denotes a radius of 1 Mpc at $z = 0.9$ centred on the cluster. The solid white circle in the lower left represents the effective FWHM of the point spread function in these beam-smoothed images. As in the X-ray, the cluster lies below the S/N threshold for detection, allowing only a 95 per cent CL upper mass limit of 3.9×10^{14} M$_\odot$, see Section 4.

cluster discussed here. We note that this cluster is ~10 Einstein radii away from the centre of A383; therefore the SL model cannot be used for the magnification estimate, but only to check consistency with our WL analysis of A383 in the region of overlap (around 0.7–1 arcmin in radius; see fig. 5 in Zitrin et al. 2011b).

It should be noted that these higher z structures are deduced in both 1D and 2D WL analyses, even though different approaches

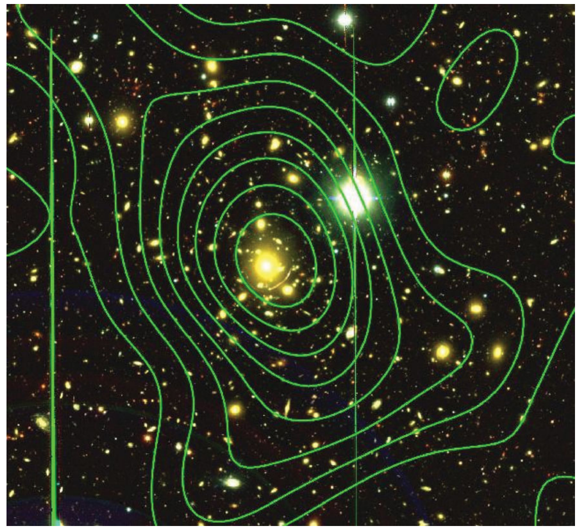

Figure 5. Contours of the dimensionless surface mass density κ smoothed with a Gaussian of full width at half-maximum (FWHM) 1.7 arcmin, superposed on the BRz' pseudo-colour image of A383. The lowest contour and the contour interval are $\Delta\kappa = 0.03$, corresponding to the 1σ reconstruction error. As can be seen, the WL analysis is sufficiently sensitive to detect a clear extension around the location of the lensed background cluster detected in the optical deep RGB colour in Fig. 2.

are employed in these. In the 1D analysis (e.g. Umetsu et al. 2011), such background structures are seen in the shape of 'dips' in the tangential shear profile, and translate to local mass excess in the lens convergence (κ) profile (see Okabe et al. 2010; see also Zitrin et al. 2011b, fig. 5). In the 2D WL analysis presented here, these will simply be seen as 2D structures in the mass distribution, as can be seen in Fig. 5.

Note also that the detection here is based on the optical data, meaning that the lensed cluster is clearly seen, and not by other means which later need further verification.

In order to calculate, or put limits on the background cluster mass, we first examine the total light by this cluster. The photometry of the 40 detected $z \sim 0.9$ cluster members add up to a total B-band luminosity of $0.84^{+0.36}_{-0.19} \times 10^{12}$ L$_\odot$ (using the luminous red galaxies templates from Benítez et al. 2009; errors include conversion from different bands), in roughly the ~2 arcmin^2 occupied by this structure in the optical. After correcting for the 14 ± 3 per cent magnification effect, this yields a total source luminosity of $0.74^{+0.32}_{-0.17} \times 10^{12}$ L$_\odot$. Adopting a typical mass-to-light ratio (M/L_B) (e.g. Zitrin et al. 2011a) of 250 ± 50 M/L_B, this translates into a total mass of $\simeq 1.84^{+0.87}_{-0.56} \times 10^{14}$ M$_\odot$ for the lensed cluster, which constitutes a lower limit on its mass, since we did not account for member galaxies lying below the detection threshold ($\simeq$26.5 AB mag in the R_c band; 5σ).

Next, we perform a 2D gravitational shear analysis of Subaru multiband ($BVR_cI_ci'z'$) data (see Zitrin et al. 2011b, on A383) to constrain the mass distribution of the $z = 0.9$ cluster. The 2D WL modelling procedure used in this work is similar to that of Watanabe et al. (2011) and Okabe et al. (2011). More details will be presented in our forthcoming paper (Umetsu et al., in preparation). From a photometric redshift (z_{ph}) selected sample of background galaxies ($z_{ph} > 0.9$, $21 < z' < 26$ AB mag), we construct a spin 2 reduced-shear field on a regular grid of 0.5×0.5 arcmin^2 independent pixels, covering a 20×20 arcmin^2 region centred on A383. We model the projected mass distribution around the $z = 0.9$ background cluster as the sum of two NFW haloes, responsible for A383 and the $z = 0.9$ cluster, each parametrized with the halo virial mass ($M_{\rm vir}$), concentration ($c_{\rm v}$) and centroid position ($x_{\rm c}$, $y_{\rm c}$). We use the Markov chain Monte Carlo technique with Metropolis–Hastings sampling to constrain the mass model with eight parameters.

From a simultaneous two-component fitting to the 2D shear data, we find $M_{\rm vir} = 1.51^{+1.45}_{-0.94} \times 10^{14}\,{\rm M}_{\odot}$ [68.3 per cent confidence limits (CLs)] for the $z = 0.9$ cluster, where other model parameters as well as the source redshift uncertainty are marginalized over. With this model, the total projected mass within a (typical virial) radius of $R = 1$ Mpc is $M_{\rm 2D} \simeq 1.9 \times 10^{14}\,{\rm M}_{\odot}$. This result is in good agreement with our optically based estimation (although the latter constitutes a lower limit).

Additionally, we use SZ measurements to deduce the gas mass, from which we estimate the total mass. Although the $z = 0.9$ cluster is not detected in the X-ray or SZ images, the SZ data do provide a constraint on the gas mass. The Bolocam SZ data were processed using the procedure described in Sayers et al. (2011); we discuss the relevant aspects of this analysis below. In particular, the data are effectively high-pass filtered in a complicated and slightly non-linear way in order to subtract noise due to fluctuations in the opacity of the atmosphere (i.e. the transfer function of the filtering depends weakly on the cluster profile). We fit an elliptical generalized NFW profile (Nagai, Kravtsov & Vikhlinin 2007; Arnaud et al. 2010) to A383, which provided a marginal fit quality (χ^2/d.o.f. = 1223/1117).[2]

Using the transfer function computed for this model, we then deconvolved the effects of noise filtering of our data to obtain an unbiased SZ image of A383. Since the filtering is somewhat non-linear, our deconvolved image of the $z = 0.9$ cluster will be slightly biased because the transfer function used for the deconvolution was determined from the profile of A383. However, even in extreme cases the bias is $<$10 per cent of the cluster peak height, which is negligible compared to our measurement noise for the $z = 0.9$ cluster.

In order to estimate the SZ signal from the $z = 0.9$ cluster, we first subtracted our best-fitting model of A383 from our unbiased SZ image. We then computed the integrated projected SZ signal within a 1 Mpc aperture (2.14 arcmin) centred on the $z = 0.9$ cluster, and found $Y_{\rm 1\,Mpc} = 0.80 \times 10^{-11}$ sr, with a statistical error of $\sigma_{Y,{\rm stat}} = 1.06 \times 10^{-11}$ sr. Restricting to physically allowed positive values of $Y_{\rm 1\,Mpc}$, this results in a 95 per cent CL upper limit of $Y_{\rm 1\,Mpc} < 2.66 \times 10^{-11}$ sr. Note that the model-subtracted A383 SZ flux within our 1 Mpc aperture is $Y_{\rm A383,model} = 1.89 \times 10^{-11}$ sr.

Using three published Y–$M_{\rm gas}$ scaling relations based on projected Y (Bonamente et al. 2008, Plagge et al. 2010 and Sayers et al. 2011), we estimate the 95 per cent CL upper limit for the gas mass of the $z = 0.9$ cluster within a spherical region of radius of 1 Mpc to be 5.1, 6.6 and $2.7 \times 10^{13}\,{\rm M}_{\odot}$, respectively. All three of these scaling relations were constrained largely (or entirely) using clusters with much higher masses, which is the likely cause of the large scatter in the derived masses. We adopt the gas mass limit derived from the Sayers et al. (2011) scaling relation, since it was calibrated using Bolocam data analysed identically to our A383 data. We note that the spread in mass limits from the three scaling relations provides an estimate of the uncertainties in the *Y*/*M* scaling.

[2] Note that we simultaneously fit, and subtracted, a point source from the NVSS catalogue at 02:48:22.09, −03:34:30.5, which we found, had a flux density of 12.8 mJy (Condon et al. 1998). This point source is approximately 5 arcmin from the centres of both A383 and the $z = 0.9$ cluster.

By assuming a typical gas mass fraction of 13 per cent (e.g. Umetsu et al. 2009), we derive a 95 per cent CL upper limit on the total mass of the $z = 0.9$ cluster of $M_{\rm SZ} < 3.9 \times 10^{14}\,{\rm M}_{\odot}$, in agreement with our previous estimates based on the luminosity and our WL analysis.

For general completeness, we repeat a similar procedure also for the X-ray data, although only a rough upper mass limit can be expected. In order to estimate the X-ray surface brightness from the $z \sim 0.9$ cluster, we consider X-ray observations retrieved from the *Chandra* archive and carried out with the AXAF CCD Imaging Spectrometer I-array (ACIS-I), namely observation ID 2320, with a total exposure time of approximately 20 ks, and use for our analysis the best-fitting triaxial model of the intracluster (IC) gas of A383 obtained by Morandi & Limousin (2011). The IC gas model generates a theoretical surface brightness map which has been subtracted from the raw brightness image. We then integrate the differential counts within a 1 Mpc aperture centred on the $z = 0.9$ cluster, translated into an X-ray luminosity by assuming a metallicity of $Z = 0.3$ solar value and the photoelectric absorption fixed to the Galactic value for the coordinates of the background cluster. This has been accomplished via fake *Chandra* spectra, where the emissivity model (MEKAL model; Kaastra 1992; Liedahl, Osterheld & Goldstein 1995) is folded through response curves (Auxiliary Response File and Response Matrix File) of the ACIS-I CCD imaging spectrometer in order to generate theoretical counts for the surface brightness. The luminosity value is obtained by rescaling the fake *Chandra* spectrum in order to reproduce the observed number of differential counts.

Given that the X-ray luminosity mildly depends also on the value of the IC gas temperature of the background cluster, which is unknown a priori, we start by assuming a guessed value of the temperature and derive the corresponding luminosity. This luminosity is then translated via the *L*–*T* relation (Morandi, Ettori & Moscardini 2007) into a global temperature, which has been used iteratively in order to estimate the X-ray luminosity and then the same global temperature for the background cluster. This process is repeated until convergence of the temperature is achieved. The luminosity is finally converted into a total mass via standard X-ray scaling relations (e.g. Morandi et al. 2007), and errors on the physical parameters were calculated via Monte Carlo randomization. We derive a 95 per cent CL upper limit on the total mass of background cluster of $M_{\rm X} < 2.5 \times 10^{14}\,{\rm M}_{\odot}$, in agreement with our previous estimates.

5 DISCUSSION AND SUMMARY

We have calculated the predicted numbers of CCLs in the ΛCDM model for different mass functions and cluster properties. According to our rather conservative estimates, only few (around three) CCLs are predicted over the full sky based on *WMAP*7 parameters, using either a PS or a ST mass function, for clusters in the mass range 1×10^{13}–$1 \times 10^{16}\,{\rm M}_{\odot}$ (for both the lens and the source). The number increases somewhat to $\sim$10 when taking into account also background groups of galaxies (down to $5 \times 10^{12}\,{\rm M}_{\odot}$), and considering different mass functions, but rises substantially to around a few dozens when taking into account possible lensing triaxiality biases, and to hundreds when considering also the WL regime.

Two CCLs were claimed a decade ago – A2152, and less significantly, MS 1008−1224, where background galaxies are obviously magnified or create a local overdensity in the image plane.

Table 1. Predicted numbers of strong CCLs over the whole sky with different cosmological parameters, mass functions, *c–M* relations and lower mass limits for the background structure. For explicit details and variations see Section 3.

Input		CCLs with PS	CCLs with ST
$M_* = 5.3 \times 10^{12}\,\mathrm{M}_\odot, A = 10, B = -0.2, C = -1$	$M_{\min} = 10^{13}\,\mathrm{M}_\odot$	$\sim$0.05	$\sim$0.2
$(\Omega_\mathrm{m}, \Omega_\Lambda, n, h, \sigma_8) = (0.266, 0.734, 0.963, 0.71, 0.801)$			
Komatsu & Seljak (2002)	$M_{\min} = 5 \times 10^{12}\,\mathrm{M}_\odot$	$\sim$0.3	$\sim$0.8
$M_* = 2 \times 10^{12}\,h^{-1}\,\mathrm{M}_\odot, A = 7.85, B = -0.081, C = -0.71$	$M_{\min} = 10^{13}\,\mathrm{M}_\odot$	$\sim$1	$\sim$2
$(\Omega_\mathrm{m}, \Omega_\Lambda, n, h, \sigma_8) = (0.258, 0.742, 0.963, 0.719, 0.796)$			
Bullock et al. (2001); Duffy et al. (2008)	$M_{\min} = 5 \times 10^{12}\,\mathrm{M}_\odot$	$\sim$3	$\sim$8
$M_* = 1.3 \times 10^{13}\,h^{-1}\,\mathrm{M}_\odot, A = 12.3, B = -0.13, C = -1$	$M_{\min} = 10^{13}\,\mathrm{M}_\odot$	$\sim$9	$\sim$17
$(\Omega_\mathrm{m}, \Omega_\Lambda, n, h, \sigma_8) = (0.258, 0.742, 0.963, 0.719, 0.796)$			
Hennawi et al. (2007)	$M_{\min} = 5 \times 10^{12}\,\mathrm{M}_\odot$	$\sim$38	$\sim$68
$M_* = 1 \times 10^{15}\,\mathrm{M}_\odot, A = 12.4, B = -0.081, C = -1$	$M_{\min} = 10^{13}\,\mathrm{M}_\odot$	$\sim$165	$\sim$260
$(\Omega_\mathrm{m}, \Omega_\Lambda, n, h, \sigma_8) = (0.258, 0.742, 0.963, 0.719, 0.796)$			
Oguri et al. (2009)	$M_{\min} = 5 \times 10^{12}\,\mathrm{M}_\odot$	$\sim$660	$\sim$940

In addition, several 'double lens' configurations were suggested or theoretically discussed before (e.g. Crawford et al. 1986; Seitz & Schneider 1994; Molinari et al. 1996; Wang & Ulmer 1997; Bertin & Lombardi 2001; Gavazzi et al. 2008). Comparison of the number of observed CCLs with theoretical predictions (see also Cooray et al. 1999) is clearly important and may add significant new insight on the evolution of the LSS in ΛCDM. This could be quite useful in light of claimed discrepancies, such as larger than predicted Einstein radii, and high concentration or disparities in the abundance of giant arcs (e.g. Hennawi et al. 2007; Broadhurst & Barkana 2008; Broadhurst et al. 2008; Sadeh & Rephaeli 2008; Puchwein & Hilbert 2009; Horesh et al. 2010; Meneghetti et al. 2010; Sereno, Jetzer & Lubini 2010; Zitrin et al. 2011a).

While inspecting lensing measurements of a sample of clusters we have noticed a lensed background clustering structure behind A383 ($z = 0.19$), in deep Subaru imaging. Photometric redshifts imply that this overdensity is at $z \sim 0.9^{+0.2}_{-0.1}$, and is clearly seen redder in an RGB colour image, and very faint in the *B* band. Our WL modelling of A383 implies a magnification of 14 ± 3 per cent of this background cluster, and a deflection angle of 22.6 ± 2.3 arcsec (so that the true location of the background cluster is $\sim$23 arcsec closer to the centre of A383).

Correcting for the magnification, the total *B*-band source luminosity is $0.74^{+0.32}_{-0.17} \times 10^{12}\,\mathrm{L}_\odot$ summed over all 40 members, which is translated into a lower limit mass estimate of $1.84^{+0.87}_{-0.56} \times 10^{14}\,\mathrm{M}_\odot$, using a typical value of $M/L_B = 250 \pm 50$. We have also analysed SZ and X-ray data, and independent WL measurements, to obtain mass estimates of $M_\mathrm{SZ} < 3.9 \times 10^{14}\,\mathrm{M}_\odot$, $M_\mathrm{X} < 2.5 \times 10^{14}\,\mathrm{M}_\odot$ (95 per cent CL upper limits) and $M_\mathrm{vir,WL} = 1.51^{+1.45}_{-0.94} \times 10^{14}\,\mathrm{M}_\odot$ [or a projected mass $M_\mathrm{2D}(<1\,\mathrm{Mpc}) \simeq 1.9 \times 10^{14}\,\mathrm{M}_\odot$], respectively. These are commensurate with our prior estimate based on the luminosity. These are also in agreement with the fact that no excess emission is seen in the SZ or X-ray images of A383 at the location of the background cluster (see Fig. 3), reflecting its probable low mass. Deeper images in the different spectral regions would be of interest to examine further the possibility that this cluster is a CCL, along with spectroscopic data for measuring the exact background cluster redshift.

In order to estimate the expected numbers of similar-mass CCLs over the whole sky, we extrapolate our results (Section 3) also to the WL regime. Assuming a flat-sky approximation, the chances for such CCLs in the weak regime grow as the ratio between the (larger) area of interest and the SL area for which we performed our calculations. For a similar, lower mass limit of $10^{14}\,\mathrm{M}_\odot$ for the background cluster, our calculations yield results in the range $\sim[2 \times 10^{-5}$ to $0.5]$ for the number of CCLs in the SL regime, depending on the chosen parameters (see e.g. Section 3 and Table 1). Taking into account the larger area for the projected location of the background cluster, we derive correspondingly a rough estimate that up to only around three similar cases maybe seen over the whole sky based on theoretical or numerical predictions, or up to $\sim$50 following observationally deduced relations. Future detections of CCLs are important, as their overall number could probe the LSS parameters, the cluster (and group) mass function, and the *c–M* relation.

ACKNOWLEDGMENTS

We thank the anonymous referee for valuable and important comments. AZ is grateful for the John Bahcall excellence prize which further encouraged this work. We thank Ian Smail, Piero Rosati, Peter Melchior and members of the CLASH team for useful comments. Work at Tel Aviv University was partly supported by the US-IL Binational Science Foundation grant 2008452, and by a grant from the British Council. AM acknowledges support by Israel Science Foundation grant 823/09. JS was partially supported by a NASA Graduate Student Research Fellowship, a NASA Post-doctoral Programme fellowship, NSF/AST-0838261, and NASA/NNX11AB07G; NC was partially supported by NASA Graduate Student Research Fellowship. This work was also partly supported by PRIN INAF 2010. Bolocam observations and analysis were also supported by the Gordon and Betty Moore Foundation. Part of this work is based on data collected at the Subaru Telescope, which is operated by the National Astronomical Society of Japan. The Chandra X-ray Observatory Center is operated by the Smithsonian Astrophysical Observatory on behalf of NASA. Bolocam was constructed and commissioned using funds from NSF/AST-9618798, NSF/AST-0098737, NSF/AST-9980846, NSF/AST-0229008 and NSF/AST-0206158.

REFERENCES

Arnaud M., Pratt G. W., Piffaretti R., Böhringer H., Croston J. H., Pointecouteau E., 2010, A&A, 517, A92

Athreya R. M., Mellier Y., van Waerbeke L., Pelló R., Fort B., Dantel-Fort M., 2002, A&A, 384, 743

Benítez N., 2000, ApJ, 536, 571

Benítez N. et al., 2004, ApJS, 150, 1
Benítez N. et al., 2009, ApJ, 691, 241
Bertin G., Lombardi M., 2001, ApJ, 546, 47
Bertin G., Lombardi M., 2006, ApJ, 648, L17
Blakeslee J. P., 2001, arXiv Astrophysics e-prints
Blakeslee J. P., Metzger M. R., Kuntschner H., Côté P., 2001, AJ, 121, 1
Bonamente M., Joy M., LaRoque S. J., Carlstrom J. E., Nagai D., Marrone D. P., 2008, ApJ, 675, 106
Broadhurst T. J., Barkana R., 2008, MNRAS, 390, 1647
Broadhurst T. et al., 2005, ApJ, 621, 53
Broadhurst T., Umetsu K., Medezinski E., Oguri M., Rephaeli Y., 2008, ApJ, 685, L9
Bullock J. S., Kolatt T. S., Sigad Y., Somerville R. S., Kravtsov A. V., Klypin A. A., Primack J. R., Dekel A., 2001, MNRAS, 321, 559
Butcher H., Oemler A., Jr, 1978, ApJ, 219, 18
Carlstrom J. E., Holder G. P., Reese E. D., 2002, ARA&A, 40, 643
Coe D., Benítez N., Sánchez S. F., Jee M., Bouwens R., Ford H., 2006, AJ, 132, 926
Coe D., Benítez N., Broadhurst T., Moustakas L. A., 2010, ApJ, 723, 1678
Comerford J. M., Natarajan P., 2007, MNRAS, 379, 190
Condon J. J., Cotton W. D., Greisen E. W., Yin Q. F., Perley R. A., Taylor G. B., Broderick J. J., 1998, AJ, 115, 1693
Cooray A. R., Holder G. P., Quashnock J. M., 1999, MNRAS, 305, L11
Crawford C. S., Fabian A. C., Rees M. J., 1986, Nat, 323, 514
Deb S., Goldberg D. M., Heymans C., Morandi A., 2010, ApJ, 721, 124
Djorgovski S., Davis M., 1987, ApJ, 313, 59
Duffy A. R., Schaye J., Kay S. T., Dalla Vecchia C., 2008, MNRAS, 390, L64
Elíasdóttir Á. et al., 2007, arXiv e-prints
Gavazzi R., Treu T., Koopmans L. V. E., Bolton A. S., Moustakas L. A., Burles S., Marshall P. J., 2008, ApJ, 677, 1046
Hennawi J. F., Dalal N., Bode P., Ostriker J. P., 2007, ApJ, 654, 714
Horesh A., Maoz D., Ebeling H., Seidel G., Bartelmann M., 2010, MNRAS, 406, 1318
Jenkins A., Frenk C. S., White S. D. M., Colberg J. M., Cole S., Evrard A. E., Couchman H. M. P., Yoshida N., 2001, MNRAS, 321, 372
Kaastra J. S., 1992, An X-Ray Spectral Code for Optically Thin Plasmas (Internal SRON-Leiden Report, updated version 2.0)
Komatsu E., Seljak U., 2002, MNRAS, 336, 1256
Kormendy J., 1977, ApJ, 218, 333
Kormendy J., Djorgovski S., 1989, ARA&A, 27, 235
Liedahl D. A., Osterheld A. L., Goldstein W. H., 1995, ApJ, 438, L115
Liesenborgs J., de Rijcke S., Dejonghe H., Bekaert P., 2007, MNRAS, 380, 1729
Limousin M. et al., 2007, ApJ, 668, 643
Limousin M. et al., 2008, A&A, 489, 23
Meneghetti M., Fedeli C., Pace F., Gottlöber S., Yepes G., 2010, A&A, 519, A90
Merten J. et al., 2011, MNRAS, 417, 333
Miyazaki S. et al., 2002, PASJ, 54, 833
Molinari E., Buzzoni A., Chincarini G., 1996, A&AS, 119, 391
Morandi A., Limousin M., 2011, preprint (arXiv:1108.0769)
Morandi A., Ettori S., Moscardini L., 2007, MNRAS, 379, 518
Nagai D., Kravtsov A. V., Vikhlinin A., 2007, ApJ, 668, 1
Navarro J. F., Frenk C. S., White S. D. M., 1996, ApJ, 462, 563 (NFW)
Newman A. B., Treu T., Ellis R. S., Sand D. J., Richard J., Marshall P. J., Capak P., Miyazaki S., 2009, ApJ, 706, 1078
Nonino M. et al., 2009, ApJS, 183, 244
Oguri M. et al., 2009, ApJ, 699, 1038
Okabe N., Takada M., Umetsu K., Futamase T., Smith G. P., 2010, PASJ, 62, 811
Okabe N., Bourdin H., Mazzotta P., Maurogordato S., 2011, ApJ, 741, 116
Plagge T. et al., 2010, ApJ, 716, 1118
Postman M. et al., 2011, preprint (arXiv:1106.3328)
Press W. H., Schechter P., 1974, ApJ, 187, 425 (PS)
Puchwein E., Hilbert S., 2009, MNRAS, 398, 1298
Rephaeli Y., 1995, ARA&A, 33, 541
Richard J. et al., 2010, MNRAS, 404, 325
Sadeh S., Rephaeli Y., 2008, MNRAS, 388, 1759
Sayers J., Golwala S. R., Ameglio S., Pierpaoli E., 2011, ApJ, 728, 39
Seitz S., Schneider P., 1994, A&A, 287, 349
Seljak U., 2000, MNRAS, 318, 203
Sereno M., Jetzer P., Lubini M., 2010, MNRAS, 403, 2077
Sheth R. K., Tormen G., 1999, MNRAS, 308, 119 (ST)
Sonnenfeld A., Bertin G., Lombardi M., 2011, A&A, 532, A37
Sunyaev R. A., Zel'dovich Y. B., 1970, Comments Astrophys. Space Phys., 2, 66
Tinker J., Kravtsov A. V., Klypin A., Abazajian K., Warren M., Yepes G., Gottlöber S., Holz D. E., 2008, ApJ, 688, 709
Umetsu K. et al., 2009, ApJ, 694, 1643
Umetsu K., Broadhurst T., Zitrin A., Medezinski E., Hsu L., 2011, ApJ, 729, 127
Valdes F. G., 1998, in Albrecht R., Hook R. N., Bushouse H. A., eds, ASP Conf. Ser. Vol. 145, Astronomical Data Analysis Software and Systems VII. Astron. Soc. Pac., San Francisco, p. 53
Wang Q. D., Ulmer M. P., 1997, MNRAS, 292, 920
Watanabe E. et al., 2011, PASJ, 63, 357
Zitrin A. et al., 2009, MNRAS, 396, 1985
Zitrin A., Broadhurst T., Barkana R., Rephaeli Y., Benítez N., 2011a, MNRAS, 410, 1939
Zitrin A. et al., 2011b, ApJ, 742, 117

This paper has been typeset from a TEX/LATEX file prepared by the author.